Calculation of General Three-Dimensional Turbulent Boundary Layers

A. K. Rastogi* and W. Rodi*
University of Karlsruhe, Karlsruhe, West Germany

A finite-difference calculation method is described for three-dimensional boundary layers in which the flow depends on all three space variables. The method employs the k-ϵ turbulence model and is applied to the following three flow situations: boundary layer on a flat plate approaching a circular cylinder mounted on the plate, boundary layer beneath the leading-edge vortex on a delta wing, and bounday layer on the upper surface of a curved duct with both zero and adverse longitudinal pressure gradients. The calculated skin friction, momentum thickness, shape factor, wall crossflow angle, and a few velocity and shear stress profiles are compared with available measurements. The results demonstrate that the calculation procedure is general and economic and that the k-ϵ turbulence model involving the assumption of an isotropic eddy viscosity provides reasonable predictions for the quantities of engineering interest.

Nomenclature

a = cylinder radius
A = finite-difference coefficient
A_k = von Karman mixing length constant
B = finite-difference coefficient
c_1, c_2, c_μ = turbulence model constants
c_f = resultant friction factor at wall, $\tau_w / \frac{1}{2}\rho U_{s\infty}{}^2$
c_{fl} = wall friction factor in the direction of freestream, $\tau_{ws\infty} / \frac{1}{2}\rho U_{s\infty}{}^2$
c_τ = dimensionless shear stress, $\tau_{s\infty} / \frac{1}{2} U_{s\infty}{}^2$
c_p = pressure coefficient, $(P - P_\infty) / \frac{1}{2}\rho U_0^2$
E = constant in the law of the wall
H = shape factor, δ_1 / θ_{11}
j = 0 for Cartesian coordinates, 1 for polar coordinates
k = turbulent kinetic energy
l_m = Prandtl's mixing length
$\dot{m}$ = entrainment rate
P = static pressure
P_k = production of turbulent kinetic energy
$R_{\theta 11}$ = Reynolds number based on momentum thickness, $U_{s\infty}\theta_{11}/\nu$
U, V, W = mean velocities in the directions x,y,z, respectively
$-\overline{uv}, -\overline{vw}$ = turbulent shear stresses (divided by ρ)
U_0 = freestream velocity at infinity
U_τ = friction velocity, $\sqrt{\tau_w/\rho}$
x,y,z = space coordinates
y_G = grid width in y direction
y^+ = normalized distance from the wall, $U_\tau y/\nu$
α = angle between resultant flow and longitudinal flow direction
β = crossflow angle
δ = boundary-layer thickness
δ_1 = displacement thickness, $\int_0^\infty (1 - U_s/U_{s\infty})\,dy$
ν, ν_t = laminar, turbulent kinematic viscosity
ϵ = dissipation rate of kinetic energy of turbulence
ρ = fluid density
θ = tangential space coordinate
θ_{11} = momentum thickness, $\int_0^\infty (U_s/U_{s\infty})[1 - (U_s/U_{s\infty})]dy$
Θ = total angle of the delta wing
τ = shear stress
σ = turbulence model constants

Subscripts

c = crossflow direction
s = streamwise direction
$s\infty$ = streamwise direction in the freestream
k = kinetic energy of turbulence
ϵ = rate of dissipation of k
x = longitudinal flow direction
R = resultant
N, S, W = north, south, west
w = wall
∞ = freestream conditions

Received Aug. 26, 1977.

Index categories: Boundary Layers and Convective Heat Transfer—Turbulent; Computational Methods.

*Research Engineer.

I. Introduction

THE great practical significance of three-dimensional turbulent boundary layers has prompted the development of various methods to predict them. A desirable feature of the methods is their applicability to a wide range of geometric configurations. In this respect, integral methods are not very successful because of difficulties in finding a general crossflow velocity profile function. Therefore, research has concentrated on the development of differential methods, and various schemes have been proposed in the literature,[1-5] with turbulence models ranging from simple mixing length formulas[5] to models employing transport equations for the two shear stress components prevailing in three-dimensional boundary layers.[3] Most of the computational schemes are restricted to cases where the flowfield can be described with two independent space variables (e.g., infinite swept wing); only a few schemes[2,4] can be used to calculate the more general cases with three independent space coordinates.

The present paper reports on the application of a method, which already has been used successfully to predict other types of flows, to three distinctly different boundary layers whose flowfield depends on three space coordinates. The method uses the k-ϵ turbulence model[6] and a simplified version of the Patankar-Spalding[7] solution procedure for three-dimensional parabolic flows. The k-ϵ model is based on the concept of an isotropic eddy viscosity and employs transport equations for the turbulent kinetic energy k and the rate of its dissipation ϵ; it is one of the most widely applied and tested turbulence models: successful calculations have been carried out for many two-dimensional wall boundary layers,[8,9] free shear flows,[10] and recirculating flows,[11-13] and recently also for three-dimensional confined flows[14-16] that

are of a more general nature than the ones considered here. The main purpose of the present study was to find out how well this generally successful model can predict the quantities of engineering interest in three-dimensional boundary layers in spite of the fact that the isotropic eddy viscosity assumption is not supported by experiments.[17-19] A further purpose of the study was to show the suitability of the versatile Patankar-Spalding[7] procedure for obtaining accurate and economic solutions for three-dimensional boundary layers in a largely different flow situation.

The present method is applied to the following three flow configurations (see Fig. 1):

1) Circular cylinder on a flat plate: The boundary layer approaching a cylinder is calculated; the freestream is assumed as potential flow around the cylinder.

2) Delta wing: The boundary layer is induced by the leading-edge vortex on a delta wing; the situation studied experimentally by East[17] is considered.

3) Curved duct: The boundary layer develops on the plane upper surface of a 60-deg curved duct; both of Vermeulen's[20] experimental cases of zero and adverse longitudinal pressure gradient are included.

Configurations 1)† and 2) were test cases at the "Trondheim Trials" of EUROMECH 60, where the performance of various three-dimensional boundary-layer calculation methods was compared[22,23]; in fact, these were the only test cases where the flow depended on three space coordinates. The present authors participated in the Trondheim Trials, and their method (described here) was the only differential method with which both of these cases were attempted. Configuration 3) was chosen as an additional test case because, in the curved duct of Vermeulen, the boundary-layer development was not dominated by pressure forces and occurs over a relatively large distance (about 100 boundary-layer thicknesses). Furthermore, extensive measurements are available for specifying boundary conditions and comparing with the predictions.

Section II introduces the calculation method and gives a detailed description of the boundary conditions used for the three configurations just listed. In Sec. III, predicted friction coefficients, shape factors, momentum thicknesses, and wall crossflow angles are presented and compared with measurements wherever possible. A few selected profiles of the mean velocity components, shear stress, and kinetic energy also are presented. Sec. IV closes the paper with concluding remarks.

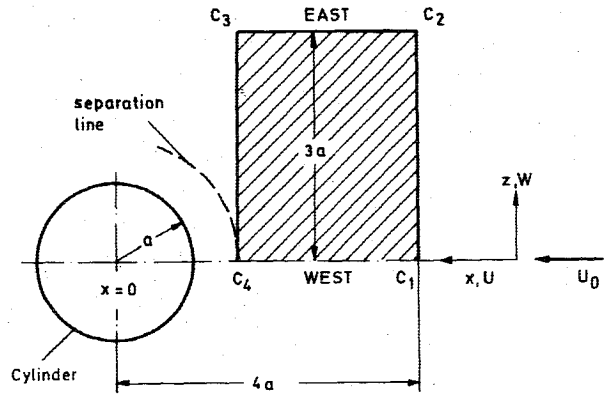

a) Circular cylinder on a flat plate

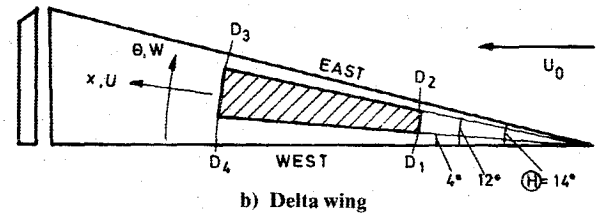

b) Delta wing

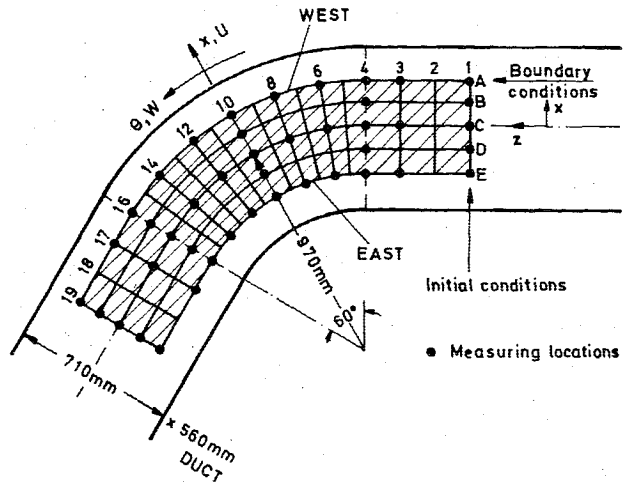

c) Curved duct

Fig. 1 Flow configurations and coordinate systems (//// calculation domain).

II. Calculation Method

A. Equations Governing the Mean Flow

The coordinate systems used in this study are shown in Fig. 1: Cartesian coordinates for the boundary layer approaching a cylinder (Fig. 1a), polar coordinates for the delta wing case (Fig. 1b), and a mixture of Cartesian coordinates (straight parts) and polar coordinates (curved part between stations 4 and 16) for the curved duct case (Fig. 1c). For both systems, the continuity and momentum equations governing the mean flow in three-dimensional boundary layers can be written as

$$\frac{1}{x^j}\frac{\partial}{\partial x}(x^j U)+\frac{\partial V}{\partial y}+\frac{\partial W}{\partial z}=0 \qquad (1)$$

$$U\frac{\partial U}{\partial x}+V\frac{\partial U}{\partial y}+W\frac{\partial U}{\partial z}-j\frac{W^2}{x}=-\frac{1}{\rho}\frac{\partial P_\infty}{\partial x}+\frac{\partial}{\partial y}(-\overline{uv}) \qquad (2)$$

$$U\frac{\partial W}{\partial x}+V\frac{\partial W}{\partial y}+W\frac{\partial W}{\partial z}+j\frac{UW}{x}=-\frac{1}{\rho}\frac{\partial P_\infty}{\partial z}+\frac{\partial}{\partial y}(-\overline{vw}) \qquad (3)$$

where $j=0$ for Cartesian coordinates, and $j=1$ as well as $\partial z=x\partial\theta$ for polar coordinates.

The preceding equations are valid only in the fully turbulent part of boundary layers, and they also are restricted to incompressible, constant property flows. As is usual for boundary layers, only the turbulent momentum flux normal to the wall is retained, and the pressure gradients are taken to be those prevailing in the freestream. As a consequence, three-dimensional boundary layers, and the equations governing them, are parabolic in both directions parallel to the wall. For example, influences can be transmitted only in the directions of increasing x and z in the region before separation of the cylinder case of Fig. 1a.

Equations (1-3) can be solved for the three mean velocity components U, V, and W provided that the turbulent shear stresses $-\overline{uv}$ and $-\overline{vw}$ and the distribution of the freestream pressure P_∞ are known. P_∞ is specified as part of the boundary conditions (see Sec. II.C); the shear stresses are determined with a turbulence model to be introduced next.

†The organizers of the Trondheim Trials did not choose exactly East and Hoxey's[21] experimental situation because there the boundary-layer development was pressure-dominated; rather the flow conditions were changed to yield a "theoretical" test case where shear forces were more important.

B. Turbulence Model

The present investigation employs the so-called k-ϵ turbulence model, which has been described in detail by Launder and Spalding.[6] The concept of an isotropic eddy viscosity is used, i.e.,

$$-\overline{uv}=\nu_t\frac{\partial U}{\partial y},\quad -\overline{vw}=\nu_t\frac{\partial W}{\partial y} \tag{4}$$

and the eddy viscosity ν_t is calculated from the Kolmogorov-Prandtl formula

$$\nu_t=c_\mu(k^2/\epsilon) \tag{5}$$

The kinetic energy of turbulence k and the rate of its dissipation ϵ are determined from the following transport equations:

$$U\frac{\partial k}{\partial x}+V\frac{\partial k}{\partial y}+W\frac{\partial k}{\partial z}=\frac{\partial}{\partial y}\left(\frac{\nu_t}{\sigma_k}\frac{\partial k}{\partial y}\right)+P_k-\epsilon \tag{6}$$

$$U\frac{\partial \epsilon}{\partial x}+V\frac{\partial \epsilon}{\partial y}+W\frac{\partial \epsilon}{\partial z}=\frac{\partial}{\partial y}\left(\frac{\nu_t}{\sigma_\epsilon}\frac{\partial \epsilon}{\partial y}\right)+c_1\frac{\epsilon}{k}P_k-c_2\frac{\epsilon^2}{k} \tag{7}$$

where P_k is the production of turbulent kinetic energy:

$$P_k=\nu_t\left[\left(\frac{\partial U}{\partial y}\right)^2+\left(\frac{\partial W}{\partial y}\right)^2\right]$$

Equations (6) and (7) are valid for both Cartesian and polar coordinate systems; centrifugal-force terms originally appearing in the polar coordinate equations have been neglected because they are of the same order of magnitude as the terms neglected by the boundary-layer approximation.

The empirical constants in Eqs. (5-7) have *not* been tuned to suit the present problems; they simply have been adopted from Launder and Spalding[6] and take the following values:

$$c_\mu=0.09,\ c_1=1.44,\ c_2=1.92,\ \sigma_k=1,\ \sigma_\epsilon=A_k/\sqrt{c_\mu}(c_2-c_1)$$

with the von Karman constant $A_k=0.4$.

A number of experiments[17-19] have shown that the resultant shear stress in three-dimensional boundary layers is not usually in the direction of the resultant velocity gradient. The use of an isotropic eddy viscosity in the k-ϵ model implies, however, that the directions of shear stress and velocity gradient are the same. It is one of the purposes of this study to find out how well the mean flow quantities can be predicted in spite of this apparently unrealistic assumption.

C. Boundary Conditions

Boundary conditions need to be specified at wall and free boundaries and at the two inflow faces of the calculation domain. At wall boundaries, use is made of the wall-function method, which is especially economical of computer time and storage because it allows a relatively coarse numerical grid near walls. Here, the grid point nearest the wall has been chosen to lie in the region of the law of the wall, i.e., $50\le y^+\le 130$, and the law of the wall then is employed to relate the velocity at this point to the wall shear stress. The following form of the law of the wall is adopted here as an extension of Spalding's[24] suggestion for two-dimensional boundary layers:

$$\frac{u_R}{u_\tau}=\frac{1}{A_k}\ln\left[Ey^+\left\{1+\frac{1}{2}\frac{y}{\rho U_\tau^2}\left(\frac{\partial P_\infty}{\partial x}\cos\alpha+\frac{\partial P_\infty}{\partial z}\sin\alpha\right)\right\}^{1/2}\right] \tag{8}$$

where U_R is the resultant velocity at the near-wall point, with the direction assumed to be that of the resultant wall shear stress; α is the angle between this direction and the x axis; E is an empirical constant for which the value 7 was adopted as suggested by the EUROMECH 60 organizers. In the law-of-the-wall region, the production P_k and dissipation ϵ of turbulent kinetic energy are assumed to be in balance. This, together with the logarithmic law for the velocity, leads to the following relations:

$$k=U_\tau^2/\sqrt{c_\mu},\quad \epsilon=U_\tau^3/A_k y \tag{9}$$

which are used as boundary conditions for k and ϵ at the near-wall point. The normal velocity component V is fixed as zero at the wall.

More refined laws of the wall have been reported in the literature[25] for three-dimensional boundary layers; it is in line with the use of the isotropic eddy viscosity concept to adopt and test the relatively simple law [Eq. (8)] in the present study. The freestream is assumed to have low turbulence; accordingly, $k=\epsilon=0$ has been specified at all freestream boundaries. The freestream velocities U_∞ and W_∞ and the conditions at the inflow faces are problem-dependent and now will be given for each of the three cases considered.

Cylinder on Flat Plate (Fig. 1a)

The calculation domain is represented by the area $C_1C_2C_3C_4$, where C_4 is the location at which separation occurs on the x axis. In this case, there is only one inflow face, namely, C_1C_2, whereas the "west" face C_1C_4 is a symmetry plane at which $W=0$ and $\partial/\partial z=0$ of all other variables. The faces C_3C_4 and C_2C_4 are outflow faces so that, because of the parabolic nature of the flow in the x and z directions, no boundary conditions need to be specified there. Conditions along C_1C_2 have been assumed corresponding to a fully developed two-dimensional turbulent boundary layer on a flat plate with $R_{\theta 11}=50{,}000$, $\theta_{11}=0.01a$, $H=1.26$, and zero crossflow. Linear $k\sim y$ profiles have been used at this inflow face, with k at the near-wall grid point specified from Eq. (9). The corresponding ϵ initial profiles were obtained from the relation‡

$$\epsilon=c_\mu^{3/4}k^{3/2}/l_m \tag{10}$$

where l_m is the Prandtl mixing length, for which a ramp function was used as suggested in Ref. 26. The freestream was assumed as inviscid flow around a circular cylinder described by

$$U_\infty-iW_\infty=U_0\{1-[a^2/(x+iz)^2]\} \tag{11}$$

These and the mean flow initial conditions at face C_1C_2 were specified by the EUROMECH 60 organizers.

Delta Wing (Fig. 1b)

The calculation domain is $D_1D_2D_3D_4$; it is restricted to the region between the primary attachment ($\theta\approx 4$ deg) and secondary separation ($\theta\approx 12$ deg) of the leading-edge vortex. Boundary conditions are not required at the outflow faces D_2D_3 and D_3D_4; in fact, the purpose of the calculation was to predict the flow at the measurement station D_3D_4, starting from the initial station D_1D_2, which was chosen 2 m upstream of D_3D_4. According to East,[17] the flow is closely conic, so that

$$\frac{\partial U_\infty}{\partial x}=\frac{\partial W_\infty}{\partial x}=\frac{\partial P_\infty}{\partial x}=0 \tag{12}$$

and the profile shapes are independent of x. The velocity profile shapes measured at D_3D_4 therefore were used to specify the profiles at the inflow boundaries D_1D_2 and D_3D_4,

‡With $l_m=A_k y$, it is easy to see that this relation corresponds to Eq. (9) near walls.

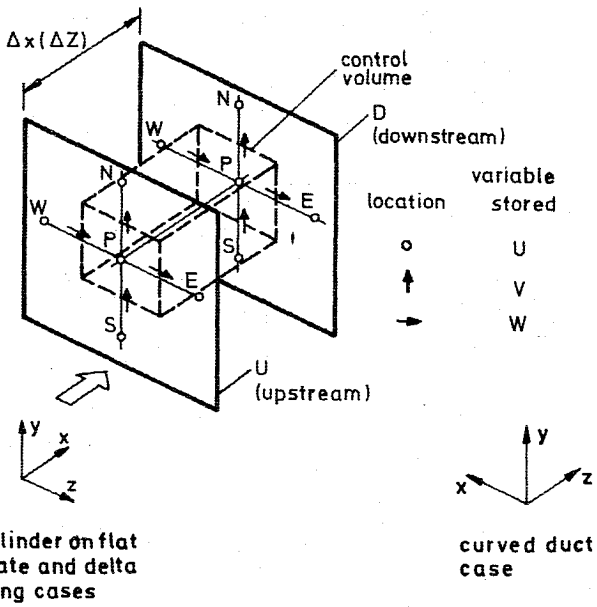

Fig. 2 Finite-difference control volume and staggered grid.

together with the assumption (suggested by the EUROMECH 60 organizers) that the starting boundary-layer thicknesses at D_1D_2 were 0.64 times the measured values at D_3D_4. The turbulence quantities at the two inflow faces were specified as described previously for the case of a cylinder on a flat plate. It should be mentioned here that the initial conditions at D_1D_2 have little influence on the predictions at D_3D_4 because the zone of dependence in this flow becomes rapidly narrower on moving upstream.[17] The measured values of U_∞ and W_∞ at D_3D_4 were taken as freestream velocities; because of Eq. (12), they are valid for the whole calculation domain. (The measured variation of the freestream pressure P_∞ with θ is shown in Fig. 8.)

Curved Duct (Fig. 1c)

The calculation domain is identical with the region covered by Vermeulen's[20] measurements; it is bounded by the measurement lines A and E and by the initial (1) and final (19) measurement stations. Here, line E and station 19 are outflow faces, so that no boundary conditions need be specified there. For the inflow faces along line A and station 1, the mean flow profiles were taken from the measurements in the following way. Power laws were chosen for the resultant mean velocity such that the measured shape factors were obtained, and the velocity components then were calculated using the measured crossflow angle profiles; between the measuring stations, the profiles were obtained by linear interpolation. At the inlet station 1, the profiles for k and ϵ were specified as described for the case of a cylinder on a flat plate. A different procedure was adopted for the inflow boundary along line A since, because of significant pressure gradients along this line, linear k-y profiles seemed inappropriate. Instead, the upstream values of k were used as boundary conditions; these values were computed after each forward step from the k value at the next grid point inside the boundary A, using the condition $\partial k/\partial x = 0$. The ϵ profiles then were determined as usual from relation (10). The freestream conditions were taken from the measured pressure distributions along the lines A to E.

D. Solution Method

Equations (1-3) and (5-7) were solved numerically for the dependent variables U, V, W, k, and ϵ with a simplified version of the solution procedure of Patankar and Spalding.[7] This procedure was developed for solving the equations in more general three-dimensional flows, which are parabolic only in one direction and whose pressure field is not known, such as flows in ducts.[14-16] For the present study, the solution procedure of Ref. 7 was simplified because the flows considered here are parabolic in two directions and do not require solving for the pressure field; also, only two momentum equations need be solved in this case. The main features of the solution method employed are as follows.

A forward-marching finite-difference scheme is used. The solution proceeds in the x direction for the cylinder-on-a-flat-plate and delta-wing cases, and in the θ direction for the curved-duct case. In the plane normal to the marching direction, a staggered grid is used, as shown in Fig. 2. The partial differential equations are integrated over the control volumes (Fig. 2) to yield linear algebraic finite-difference equations connecting the dependent variables at a downstream grid point to unknown values at the neighboring points and to known upstream quantities. If ϕ stands for the dependent variable in question, the difference equations take the following form:

$$\phi_p = A_N\phi_N + A_S\phi_S + A_W\phi_W + B \tag{13}$$

where the coefficients A and B involve only known upstream quantities. Unlike in the original procedure,[7] ϕ_p is not connected to the value ϕ_E because the flows considered here are parabolic in the west-east direction.

The finite-difference equations are solved by tridiagonal matrix algorithm traverses in the y direction, sweeping from the west face toward the east face. Only a single sweep was necessary for each variable in this case, whereas the presence of ϕ_E in the difference equation (13) would have necessitated several sweeps. The momentum equations (2) and (3) were solved first for U and W; the velocity component V then was obtained from the continuity equation (1). The next step was to use U, V, and W in the solution for k and ϵ from Eqs. (6) and (7).

The grid normal to the wall expanded with the boundary-layer growth. The grid expansion was specified from the experiments in the cases of delta wing and curved duct. For the case of the cylinder on a flat plate, the expansion was calculated from

$$\rho U_\infty \frac{dy_G}{dx} - \rho V_\infty = \dot{m} \tag{14}$$

where y_G is the grid width in the y direction, and the entrainment $\dot{m}$ was calculated as suggested for two-dimensional boundary layers in Ref. 26.

A 20×20 cross-stream grid was found to provide grid-independent solutions. The calculations were started with small forward steps of 1% of the maximum boundary-layer thickness and gradually were increased to a maximum value of 25% of the local maximum boundary-layer thickness. The computing time required per equation solved, per grid node, and per forward step was 46×10^{-3} s on a UNIVAC 1108. A typical time for one complete calculation was 6 min. 35K words of computer memory were needed.

III. Presentation and Discussion of Results

A. Cylinder-on-Flat-Plate Case

The calculated variation with x of the momentum thickness θ_{11}, the shape factor H, and the crossflow angle at the wall β_w is shown for various distances from the symmetry plane in Figs. 3-5, respectively. With the Cartesian coordinate system used, the boundary-layer calculation could be carried out only up to $x/a = -1.54$, where separation occurred on the symmetry plane, as can be seen from Fig. 4. Therefore, only the point of separation on the x axis can be predicted but not the separation line in the x-z plane, as sketched in Fig. 1a. According to Spalding,[27] this limitation can be overcome by using a polar coordinate system with the origin at the center of the cylinder and by marching in the tangential direction

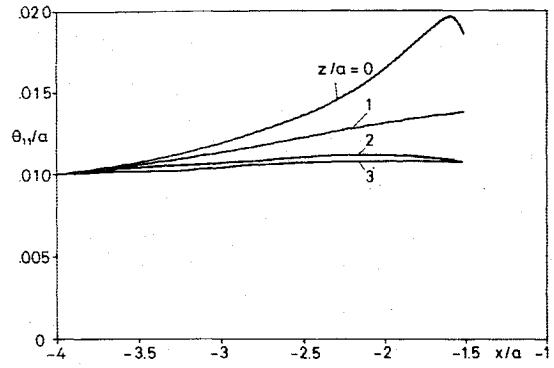

Fig. 3 Calculated momentum thickness for cylinder on flat-plate case.

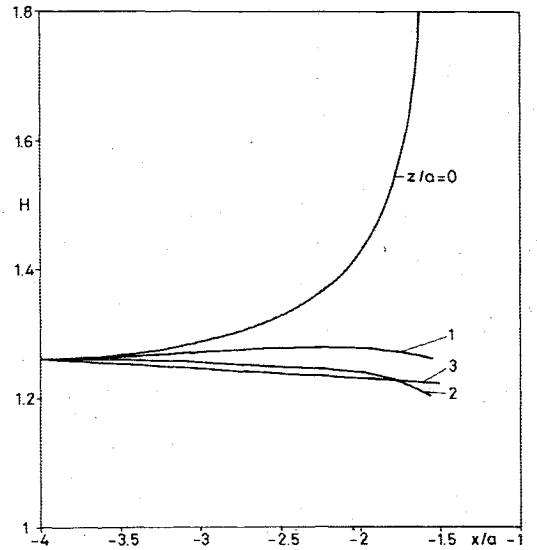

Fig. 4 Calculated shape factor for cylinder on flat-plate case.

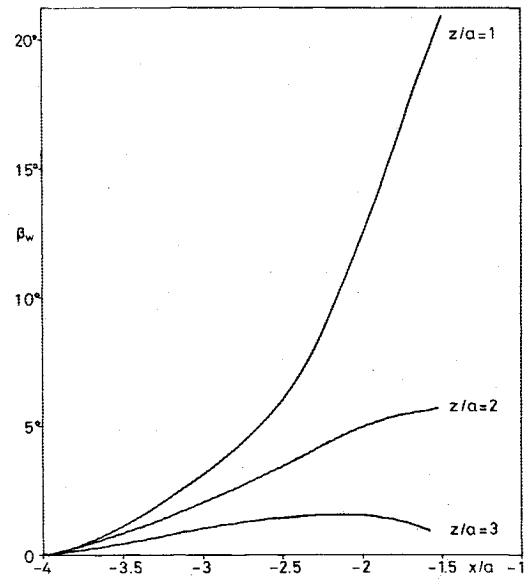

Fig. 5 Calculated wall crossflow angle for cylinder on flat-plate case.

around the cylinder. This approach, which requires employment of the original solution procedure of Ref. 7 to allow for recirculation in the x-y plane, was not attempted in the present study, however.

The behavior of θ_{11} and H on the symmetry plane ($z=0$) is as expected in a flow with strong adverse pressure gradient.

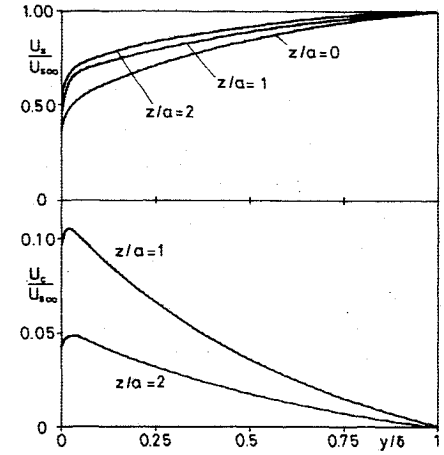

Fig. 6 Calculated streamwise and crossflow velocity profiles for cylinder on flat-plate case (at $x/a=-2$).

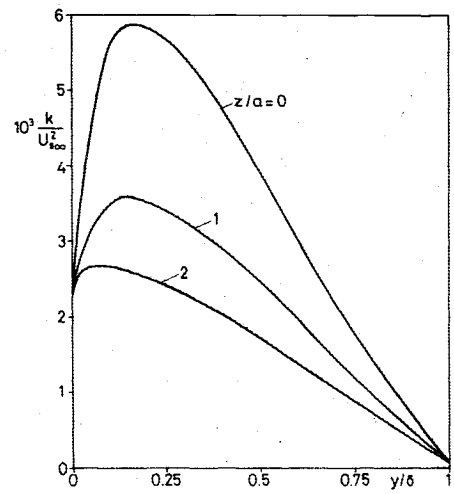

Fig. 7 Calculated turbulent kinetic energy profiles for cylinder on flat-plate case (at $x/a=-2$).

Off the symmetry plane, the flow is accelerated around the cylinder, which explains the decrease in H. In the boundary layer, and particularly near the wall, the streamline curvature is larger than in the freestream, because the same pressure gradient has to be balanced, largely by centrifugal forces, at lower velocities. As can be seen from Fig. 5, this effect is strongest near the symmetry plane, where the freestream curvature is strongest. At the symmetry plane itself, the curvature of both freestream and boundary-layer flow is, of course, zero, so that the crossflow angle is zero.

Figure 6 shows some representative profiles of the streamwise and crossflow velocity components. The effect of the increasing pressure gradient toward the plane of symmetry is manifested by the fact that the streamwise velocity profiles become less full. The crossflow velocity has its maximum very close to the wall; the shape of the profiles agrees well with recent measurements in a similar flow situation by Dechow and Felsch.[19] As expected from two-dimensional boundary-layer measurements, the level of the turbulent kinetic energy shown in Fig. 7 is higher in regions with larger pressure gradients, and the maximum is further away from the wall. The predictions are again in qualitative agreement with the measurements of Ref. 19.

B. Delta-Wing Case

The predictions are compared with the measurements of East[17] at section D_3D_4 across the wing (see Fig. 1b). The imposed pressure distribution shown in Fig. 8 illustrates that, starting from the attachment point ($\theta/\Theta \approx 0.29$), the flow is

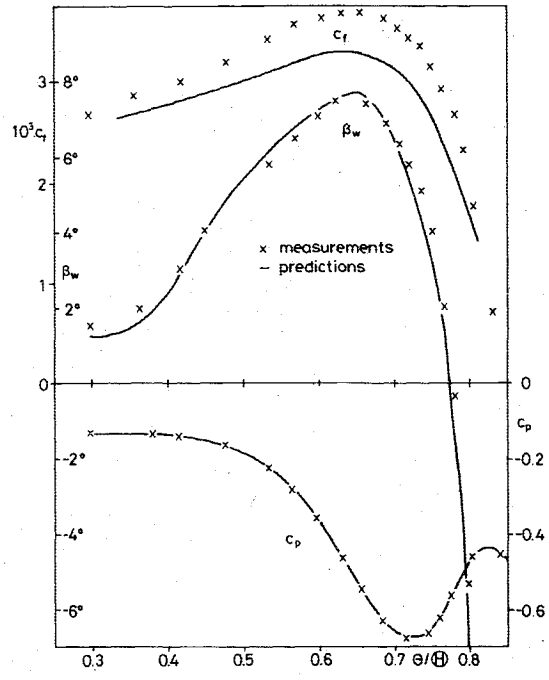

Fig. 8 Friction factor, wall crossflow angle, and freestream pressure variation across the delta wing.

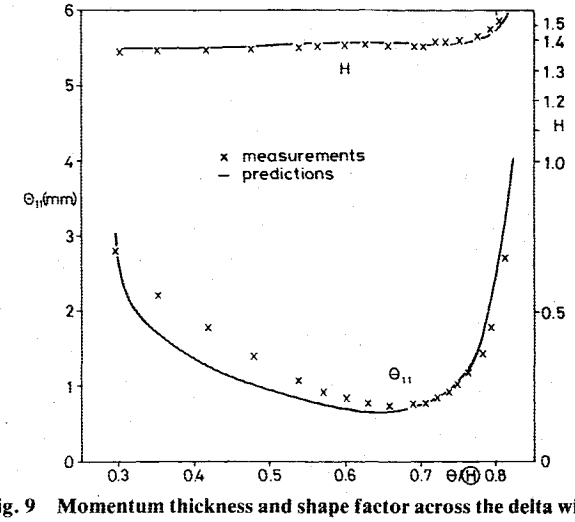

Fig. 9 Momentum thickness and shape factor across the delta wing.

accelerated toward the leading edge and then is retarded until it separates at $\theta/\Theta \approx 0.85$. The predicted variation of the wall crossflow angle β_w and the shape factor H agrees very well with the experiments, as is shown in Figs. 8 and 9; in particular, the prediction method can cope well with the change in crossflow direction. The friction factor c_f and the momentum thickness θ_{11} also are shown in Figs. 8 and 9, respectively. General agreement is again fairly good, but c_f is somewhat underpredicted, mainly in the region where the boundary-layer thickness is small, and θ_{11} is underpredicted in the accelerating flow region. These discrepancies may be due to the limited accuracy of the simple law of the wall employed.

Figure 10 presents streamwise and crossflow velocity profiles at two angles θ before and after the position of change in crossflow direction. The predicted profiles agree fairly well with the measured ones. Profiles of shear stress in the direction of the external flow are displayed for three angles θ in Fig. 11; at the two smaller angles θ, the predicted profiles are compared with values determined by East[17] from his velocity measurements via the momentum equations. The good agreement is not surprising in view of the agreement of

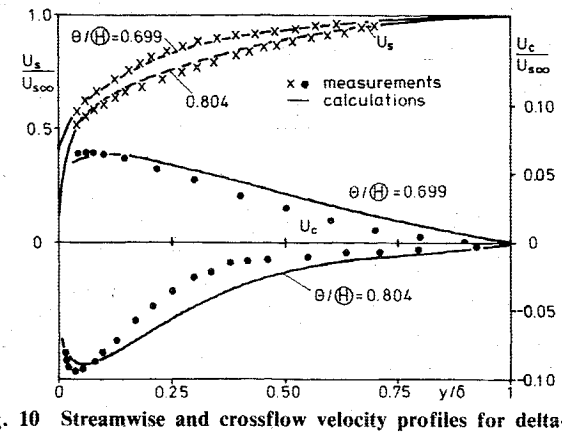

Fig. 10 Streamwise and crossflow velocity profiles for delta-wing case.

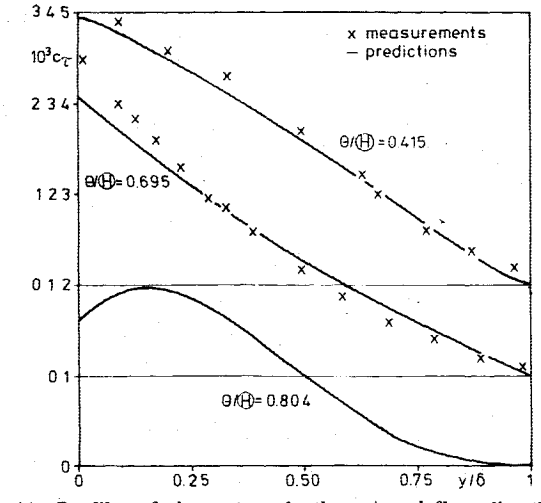

Fig. 11 Profiles of shear stress in the external flow direction for delta-wing case.

integral parameters. The predicted profile at $\theta/\Theta = 0.695$ is somewhat too low near the wall, which is consistent with the low c_f value shown in Fig. 8. The fact that there is good agreement further away from the wall supports the notion that the underprediction is caused by the law of the wall. At $\theta/\Theta = 0.804$, where values determined from experiments are not available, the shear stress has its maximum off the wall, as is characteristic near separation.

C. Curved-Duct Case

Figures 12-15 show the variation of c_{fl}, θ_{11}, H, and β_w along the lines B, C, and D (see Fig. 1c) for both the zero and adverse longitudinal pressure gradient cases studied experimentally by Vermeulen.[20] The somewhat wavy nature of the predictions, particularly of β_w in Fig. 15b, is due to the linear interpolation used in obtaining the freestream conditions and the boundary condition along line A from measured values at the points shown in Fig. 1c. A more refined interpolation scheme might have avoided these irregularities.

The predicted friction factors shown in Fig. 12 are in good agreement with the measured values over most of the flow. The initial values are somewhat low; this is because the initial profiles along station 1 were not actually the measured profiles but rather power laws that gave the correct shape factor. A more elaborate scheme of reading in the measured profiles is necessary to produce also the correct initial c_{fl} values. However, the influence of the low initial c_{fl} values on the downstream predictions is small. Figure 12b shows that, for the case with adverse pressure gradient, the reduction of c_{fl} near separation is predicted correctly.

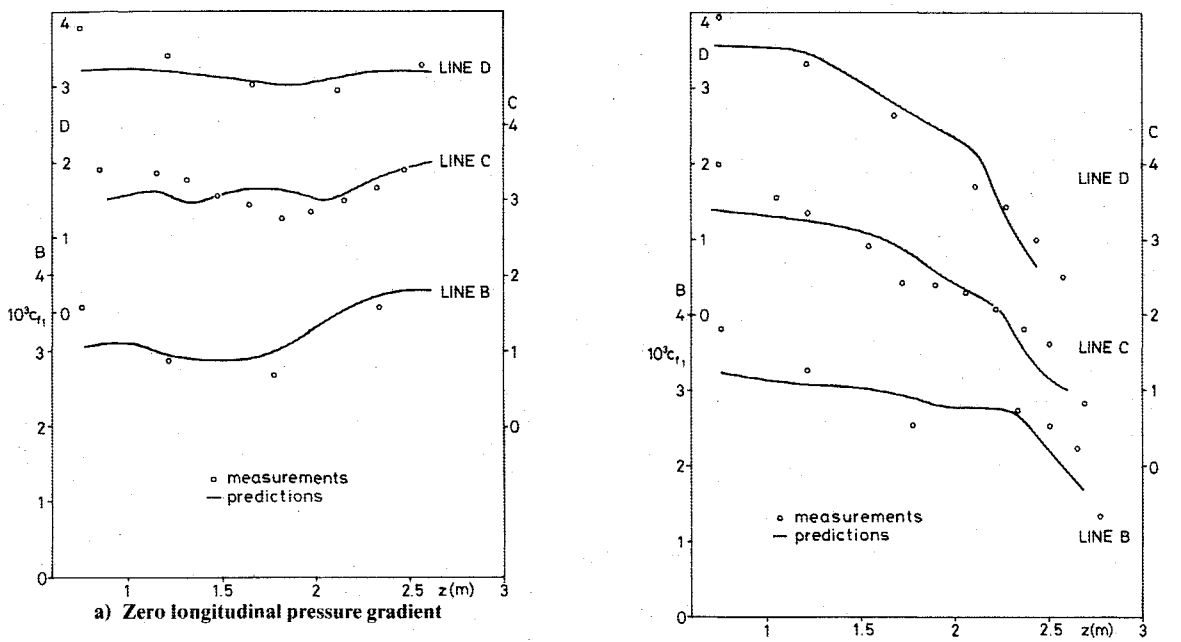

a) Zero longitudinal pressure gradient

b) Adverse longitudinal pressure gradient

Fig. 12 Streamwise friction factor for curved-duct case.

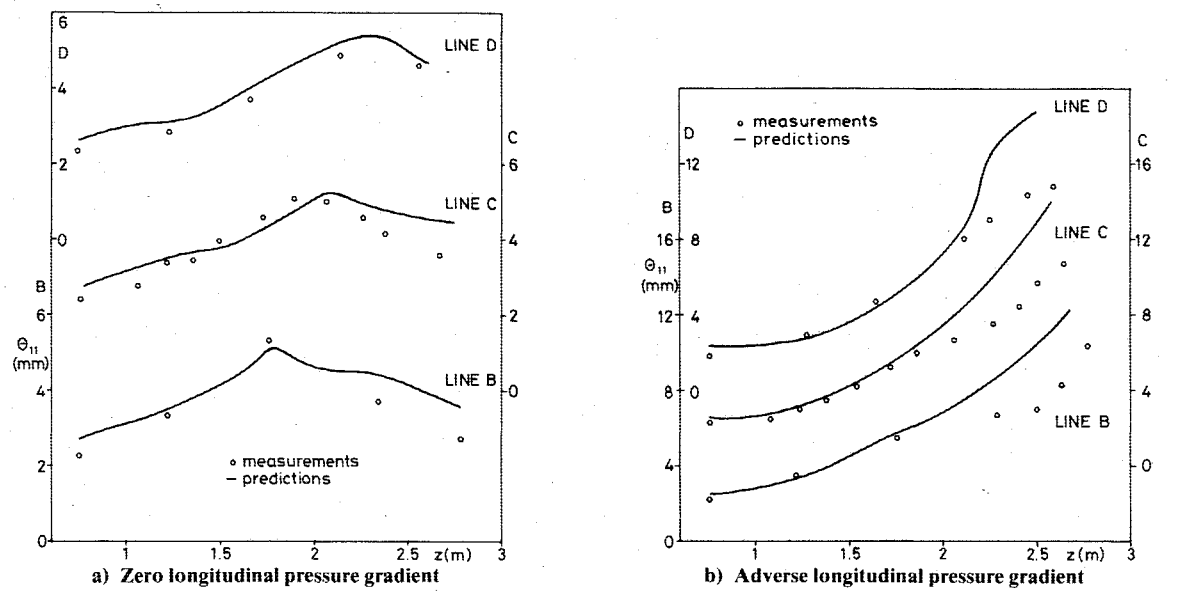

a) Zero longitudinal pressure gradient

b) Adverse longitudinal pressure gradient

Fig. 13 Momentum thickness for curved-duct case.

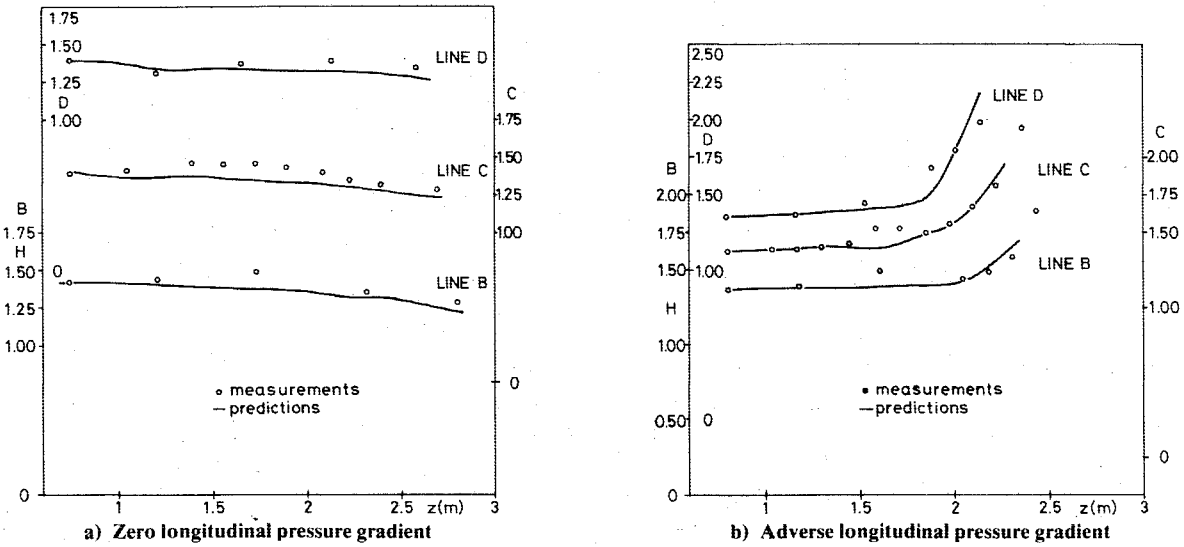

a) Zero longitudinal pressure gradient

b) Adverse longitudinal pressure gradient

Fig. 14 Shape factor for curved-duct case.

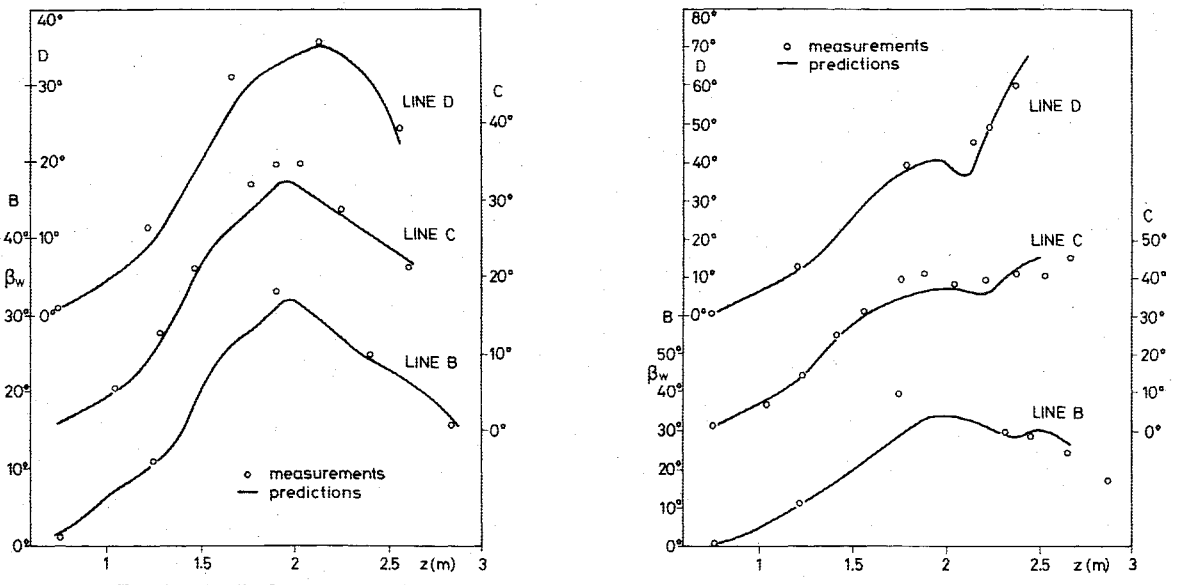

a) Zero longitudinal pressure gradient b) Adverse longitudinal pressure gradient

Fig. 15 Wall crossflow angle for curved-duct case.

The predicted momentum thickness θ_{11} shown in Fig. 13 is also in generally good agreement with Vermeulen's data; only near the separation in the case with adverse pressure gradient does the predicted θ_{11} rise too quickly (Fig. 13b). The shape factor H, on the other hand, shows the correct approach toward separation (Fig. 14b). In the case with zero longitudinal pressure gradient, H varies little over the flowfield (Fig. 14a). The measured behavior of the crossflow angle at the wall β_w is generally well reproduced by the calculations (Fig. 15) if we ignore the wiggles discussed already. In the case with adverse pressure gradient, the predicted β_w is of the order of 15% too low around station 10, but the approach toward separation is well predicted.

In the case with adverse pressure gradient, the calculation stopped at station 18 because separation occurred on line E. In the experiments, separation also was observed to occur first on line E and approximately at station 18. Calculations with Nash's[2] method reported in Ref. 20 yielded separation already between stations 16 and 17. On the whole, the present predictions are at least as good as Nash's differential and Smith's integral method calculations reported in Ref. 20.

IV. Conclusions

From the previous section, one may conclude that the present prediction method provides generally satisfactory results for all of the three flow configurations considered. Direct comparison with experiments was not possible in the case of the cylinder on a flat plate; but the results appear reasonable in every respect, so that the method can be trusted to predict the flow well up to the station where separation occurs at the symmetry plane. For the delta-wing and curved-duct cases, there is, on the whole, fairly good agreement with experimental data; modest disagreement is limited to rather small areas of the flows and could be reduced partly by more refined specifications of boundary and initial conditions. Thus the k-ϵ turbulence model, which proved successful in predicting a large variety of other flows, appears to provide fairly good mean flow predictions also for three-dimensional boundary layers. The use of an isotropic eddy viscosity, which, according to a number of experiments, is unrealistic and leads to incorrect shear stress directions, does not impair seriously the predictions of quantities of engineering interest. A similar conclusion can be inferred from Wheeler and Johnston's[28] study on the performance of various methods applied to the special type of three-dimensional boundary layers that depend on two space variables only. There may be situations in which the isotropic eddy viscosity assumption is too simple; but the evidence so far suggests that, in most cases, it is adequate for engineering purposes. A similar statement seems justified for the use of the relatively simple law of the wall used in this study.

The simplified version of Patankar and Spalding's solution procedure could be adopted without difficulty for all three configurations considered. The procedure proved to be flexible and economic and thus, together with the k-ϵ model, provides a powerful tool for predicting general boundary layers where the flowfield depends on all three space variables.

Acknowledgments

The authors would like to thank D. B. Spalding for helpful suggestions on this work. The numerical calculations were carried out on the UNIVAC 1108 computer at the University of Karlsruhe using a modified version of the program STABLE of CHAM Ltd., London, which is based on the solution algorithm of Ref. 7.

References

[1] Nash, J. F., "The Calculation of Three-Dimensional Turbulent Boundary Layers in Incompressible Flow," *Journal of Fluid Mechanics*, Vol. 37, 1969, pp. 625-642.

[2] Nash, J. F., "An Explicit Scheme for the Calculation of Three-Dimensional Turbulent Boundary Layers," American Society of Mechanical Engineers, Paper 71-Fe-19, 1971.

[3] Bradshaw, P., "Calculation of Three-Dimensional Turbulent Boundary Layers," *Journal of Fluid Mechanics*, Vol. 46, 1969, pp. 417-445.

[4] Cebeci, T., "A General Method for Calculating Three-Dimensional Incompressible Laminar and Turbulent Boundary Layers, II. Three-Dimensional Flows in Cartesian Coordinates," Douglas Aircraft Co., Rept. MDC 36517, March 1974.

[5] Mellor, G., "Incompressible, Turbulent Boundary Layers with Arbitrary Pressure Gradients and Divergent or Convergent Cross Flows," *AIAA Journal*, Vol. 5, Sept. 1967, pp. 1570-1579.

[6] Launder, B. E. and Spalding, D. B., "The Numerical Calculation of Turbulent Flows," *Computer Methods in Applied Mechanics and Engineering*, Vol. 3, 1974, pp. 269-289.

[7] Patankar, S. V. and Spalding, D. B., "A Calculation Procedure for Heat, Mass and Momentum Transfer in Three-Dimensional Parabolic Flows," *International Journal of Heat and Mass Transfer*, Vol. 15, 1972, pp. 1787-1805.

[8] Jones, W. P. and Launder, B. E., "The Prediction of Laminarization with a Two-Equation Model of Turbulence," *In-*

ternational Journal of Heat and Mass Transfer, Vol. 15, 1972, pp. 301-314.

[9]Singhal, A. K. and Spalding, D. B., "Predictions of Two-Dimensional Boundary Layers with the Aid of the k-ϵ Model of Turbulence," Imperial College, London, Rept. HTS/75, 15, May 1975.

[10]Launder, B. E., Morse, A., Rodi, W., and Spalding, D. B., "Prediction of Free Shear Flows—A Comparison of Six Turbulence Models," *Proceedings of the Langley Conference on Free Turbulent Shear Flows*, NASA SP-321, 1973.

[11]Elgobashi, S. E. and Pun, W. M., "A Theoretical and Experimental Study of Turbulent Diffusion Flames in Cylindrical Furnaces," *Proceedings of the 15th Symposium on Combustion*, 1974.

[12]Gosman, A. D., Khalil, E. E., and Whitelaw, J. H., "The Calculation of Two-Dimensional Turbulent Recirculating Flows," *Proceedings of the Symposium on Turbulent Shear Flows*, Pennsylvania State Univ., April 1977.

[13]Durst, F. and Rastogi, A. K., "Theoretical and Experimental Investigations of Turbulent Flows with Separation," *Proceedings of the Symposium on Turbulent Shear Flows*, Pennsylvania State Univ., April 1977.

[14]Sharma, D., "Turbulent Convective Phenomena in Straight, Rectangular-Sectioned Diffusers," Ph.D. Thesis, Univ. of London, 1974.

[15]Patankar, S. V., Pratap, V. S., and Spalding, D. B., "Prediction of Turbulent Flow in Curved Pipes," *Journal of Fluid Mechanics*, Vol. 67, Pt. 3, 1975, pp. 583-596.

[16]McGuirk, J. and Spalding, D. B., "Mathematical Modelling of Thermal Pollution in Rivers," *Proceedings of the International Conference on Mathematical Models for Environmental Problems*, Southampton, England, 1975.

[17]East, L. F., "Measurements of the Three-Dimensional Incompressible Turbulent Boundary Layer Induced on the Surface of a Slender Delta Wing by the Leading Edge Vortex," Aeronautical Research Council, R&M 3768, 1973.

[18]Elsenaar, A. and Boelsma, S. H., "Measurements of the Reynolds Stress Tensor in a Three-Dimensional Turbulent Boundary Layer under Infinite Swept Wing Conditions," National Aerospace Lab., Netherlands, NL R TR 74095 U, 1974.

[19]Dechow, R. and Felsch, K. O., "Measurements of the Mean Velocity and the Reynolds Stress Tensor in a Three-Dimensional Turbulent Boundary Layer Induced by a Cylinder Standing on a Flat Wall," *Proceedings of the Symposium on Turbulent Shear Flow*, Pennsylvania State Univ., April 1977.

[20]Vermeulen, A. J., "Measurements of Three-Dimensional Turbulent Boundary Layers," Ph.D. Thesis, Univ. of Cambridge, 1971.

[21]East, L. F. and Hoxey, R. P., "Low Speed Three-Dimensional Turbulent Boundary Layer Data," Pts. 1 and 2, Aeronautical Research Council, R&M 3653, 1969.

[22]Fanneløp, T. K. and Krogstad, P. A., "Three-Dimensional Turbulent Boundary Layers in External Flows, Report on EUROMECH 60," *Journal of Fluid Mechanics*, Vol. 71, 1975, pp. 815-826.

[23]East, L. F., "Computation of Three-Dimensional Turbulent Boundary Layers, EUROMECH 60, Trondheim 1975," Aeronautical Research Inst. of Sweden, FFA TN AE-1211, Sept. 1975.

[24]Spalding, D. B., "A General Computer Program for Two-Dimensional Boundary Layer Problems," Imperial College, London, Rept. HTS/73/48, Sept. 1973.

[25]Van den Berg, B., "A Three-Dimensional Law of the Wall for Turbulent Shear Flows," *Journal of Fluid Mechanics*, Vol. 70, 1975, pp. 149-160.

[26]Patankar, S. V. and Spalding, D. B., *Heat and Mass Transfer in Boundary Layers*, 2nd ed., Intertext, London, 1970.

[27]Spalding, D. B., private communication.

[28]Wheeler, A. J. and Johnston, J. P., "An Assessment of Three-Dimensional Turbulent Boundary Layer Prediction Methods," *Transactions of ASME, Journal of Fluid Engineering*, Sept. 1973, pp. 415-421.